Coexisting Domains in the Plasma Membranes of Live Cells Characterized by Spin-Label ESR Spectroscopy

Musti J. Swamy, Laura Ciani, Mingtao Ge, Andrew K. Smith, David Holowka, Barbara Baird, and Jack H. Freed
Department of Chemistry and Chemical Biology, Cornell University, Ithaca, New York 14853

ABSTRACT   The importance of membrane-based compartmentalization in eukaryotic cell function has become broadly appreciated, and a number of studies indicate that these eukaryotic cell membranes contain coexisting liquid-ordered (L_o) and liquid-disordered (L_d) lipid domains. However, the current evidence for such phase separation is indirect, and so far there has been no direct demonstration of differences in the ordering and dynamics for the lipids in these two types of regions or their relative amounts in the plasma membranes of live cells. In this study, we provide direct evidence for the presence of two different types of lipid populations in the plasma membranes of live cells from four different cell lines by electron spin resonance. Analysis of the electron spin resonance spectra recorded over a range of temperatures, from 5 to 37°C, shows that the spin-labeled phospholipids incorporated experience two types of environments, L_o and L_d, with distinct order parameters and rotational diffusion coefficients but with some differences among the four cell lines. These results suggest that coexistence of lipid domains that differ significantly in their dynamic order in the plasma membrane is a general phenomenon. The L_o region is found to be a major component in contrast to a model in which small liquid-ordered lipid rafts exist in a 'sea' of disordered lipids. The results on ordering and dynamics for the live cells are also compared with those from model membranes exhibiting co-existing L_o and L_d phases.

INTRODUCTION

Considerable evidence has accumulated in recent years to support the view that lipid-dependent plasma membrane heterogeneity plays important roles in cellular processes including signal transduction and membrane trafficking. Microdomains of ordered lipids, commonly called lipid rafts, are hypothesized to be platforms for performing these biological functions (1). These microdomains are enriched in sphingolipids, cholesterol, and phospholipids containing mostly saturated fatty acid chains and proteins anchored to the membrane with saturated lipids, as determined by their insolubility in certain nonionic detergents at 4°C (2). The functional relevance associated with these microdomains is their capacity for selective segregation of proteins. Thus some membrane proteins with compatible membrane-anchoring structures preferentially partition into these environments (e.g., Src kinases), just as others with incompatible structures partition out (e.g., transmembrane phosphatases), and this enables critical interactions to occur in a regulated manner (e.g., after cross-linking specific receptors that localize to rafts) (3,4). However, despite widespread attention, lipid rafts (referred to below as rafts) have been elusive to experimental definition because of the compositional heterogeneity of lipids and proteins and their dynamic nature in the living cell. In particular, it has not been possible to visualize rafts on plasma membranes of unstimulated cells within the limits of optical resolution at the same time that a large fraction of the plasma membrane appears to be 'raft-like' based on detergent insolubility and other biochemical criteria (5,6).

Consistent with the view that there are more and less ordered regions of the plasma membrane, several fluorescence studies have demonstrated that liquid-ordered (L_o) and liquid-disordered (L_d) phases can coexist in giant unilamellar vesicles composed of cholesterol and other defined lipids or isolated plasma membrane lipids (7–10). Synthetic vesicles that have a lipid composition similar to that of the rafts are largely detergent insoluble (11), suggesting that the rafts have an L_o phase structure. However, the concern remains that detergents could reorganize the structure of cell membranes and result in coalescence of lipid rafts, and even could create rafts that otherwise do not exist (12).

Electron spin resonance (ESR) offers the opportunity to measure directly the phase behavior of plasma membranes. Previous studies were carried out on detergent resistant membranes (DRM; (13)) and plasma membrane vesicles (PMV; (14)) derived from RBL-2H3 mast cells that have served as a model system for raft-mediated transmembrane signaling (15). These measurements yielded values for the order parameters (S_0) and rotational diffusion coefficients ($R_\perp$) of phosphatidylcholine (PC) probes with spin-labeled acyl chains and showed the detergent-resistant membranes to have properties of the L_o phase (13). Coexistence of two lipid populations with L_o and L_d phases was revealed for the PMV, and the L_d component disappeared after the proteins were extracted (14).

In this work we carried out ESR studies on living RBL-2H3, COS7, NIH-3T3, and CHO cells, thereby avoiding any complications caused by cellular disruption or alteration of membrane organization. The results provide for the first time, to our knowledge, direct evidence for the presence of two distinctive lipid populations that differ significantly in their dynamic order in the plasma membrane of live cells. Consistent with the previous results obtained with PMV, we find that the L_o membrane is a major component that appears to predominate in the live cells. This would be consistent with a model wherein there is a continuous L_o phase (16), within which there are small regions of L_d phase rather than the reverse model that was previously suggested of small discrete ''rafts'' of L_o phase existing in a continuous 'sea' of L_d phase (1,2,5,6). We also provide a comparison of the live cell results with coexisting L_o and L_d phases in the model ternary membrane system consisting of SPM/DOPC/Chol.

MATERIALS AND METHODS

Materials

The spin labels 5PC, 7PC, 10PC, 12PC, 14PC, and 16PC were purchased from Avanti Polar Lipids (Alabaster, AL). BODIPY-GM1 was obtained from Molecular Probes (Eugene, OR).

Cell cultures

RBL-2H3 (17) and Chinese hamster ovary (CHO) (18) cells were grown adherent in either 75- or 150-cm^2 flasks as described previously. NIH-3T3 and COS-7 cells were grown adherent in 10-cm dishes under conditions described by the American Type Culture Center. All cells were harvested using EDTA buffer (135 mM NaCl, 5 mM KCl, 20 mM Hepes, and 1.5 mM EDTA, pH 7.4) and resuspended in buffered saline solution (BSS; 135 mM NaCl, 5 mM KCl, 1.8 mM CaCl$_2$, 5.6 mM glucose, 20 mM HEPES, pH 7.4) containing 1 mg/ml bovine serum albumin (BSS/BSA) and used for the ESR experiments as described below. Cell viability was assessed by Trypan blue staining.

Labeling live cells with spin-labeled lipids and ESR spectroscopy

Cells were labeled with a series of spin-labeled PCs, nPC, bearing the nitroxide moiety at C5, C7, C10, C12, C14, and C16 on the sn-2 acyl chain (Fig. 1). The methodology is very similar to that for incorporating fluorescently labeled lipids, such as DiIC$_{18}$, into the plasma membranes of these cells (19). The nPC spin-labeled lipids were incorporated into the plasma membranes of RBL-2H3 cells, CHO cells, NIH-3T3 cells, or COS-7 cells in the following way: ~1.5–3.0 × 10^6 cells were suspended in ~1.5 mL of cold BSS/BSA and 30 μL of the spin-labeled lipid in methanol was added from a 1-mM stock solution. The sample was mixed quickly, allowed to stand at room temperature for 1 min, and then kept on ice for 1 min. The cells were then pelleted by centrifugation (800 rpm for 3–5 min at 5°C), resuspended in 1 mL of the same buffer, and then pelleted again. We confirmed that no ESR signal was detected from the supernatant after each centrifugation, indicating that no spin-label molecules were trapped in or bound to BSA in the buffer and that all the ESR signal was due to spin labels incorporated into the cells. The resulting cell pellet was suspended in ~100 μL of cold BSS, transferred to a 1.8-mm outside diameter glass capillary, and pelleted again by centrifugation. The capillary was used immediately for ESR spectral measurement. To ensure that the spin labels incorporated into the plasma membrane are not internalized, the labeling was carried out at low temperature (5°C–10°C), where endocytosis is drastically reduced, if not totally arrested (19,20).
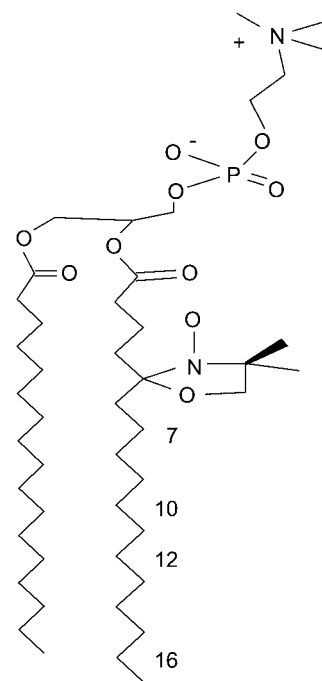

FIGURE 1 Structures of the spin-labeled PCs. The structure shown is that of 5PC, with the doxyl spin label attached to the C5 of the sn-2 acyl chain. Other spin labels, namely 7PC, 10PC, 12PC, and 16PC have the doxyl group attached to C7, C10, C12, and C16, respectively, of the sn-2 acyl chain.

ESR spectra were recorded on a Bruker (Billerica, MA) EMX ESR spectrometer at 9.3 GHz within 30–60 min of labeling. Spectra were recorded at temperatures 5°C, 15°C, 25°C, and 37°C; for each temperature a new sample of freshly labeled cells was used in most cases. All experiments on the four different cell types were repeated at least two times to confirm reproducibility. After the ESR measurements, cell viability was tested by Trypan blue stain, and the results from samples exhibiting >95% viability were analyzed further.

Preparation of model membranes

Spin-labeled lipid dispersions consisting of sphingomyelin (SPM), dioleoylphosphatidylcholine (DOPC), and cholesterol (Chol) were prepared as follows. Measured volumes of lipid stocks (lipids dissolved in chloroform) and the spin-label stock were dispensed into glass sample tubes using a Hamilton syringe to give the desired lipid compositions. The spin labels used were 5, 7, 10, 12, 14, and 16PC. The concentration of spin label in the lipid dispersion was <0.5 mol % of the total lipids. These lipid-chloroform solutions were then converted to lipid-buffer suspensions by rapid solvent exchange (21). The buffer used was 50 mM Tris, 10 mM NaCl, and 0.1 mM EDTA at pH 7.0. The samples were placed in the dark at room temperature to reach equilibrium. After several days the samples were centrifuged, and the pellets were transferred to 1.5–1.8-mm-diameter × 100-mm-length glass capillaries. The ends of the capillaries were flame sealed.

Determination of partition coefficients of PC spin labels between coexisting L_d and L_o phases in the model membranes

The phase diagram for ternary lipid mixtures of SPM/DOPC/Chol has previously been studied (22–24). The phase diagram at 22°C (22), for the region of a coexistence of L_o and L_d phases, is shown in Fig. 2 A. Lipid dispersions of SPM/DOPC/Chol containing 0.5 mol % 16PC were prepared

with compositions that lie along the phase boundary (PB) of the coexistence region of the L_o and L_d phases; these 12 compositions are marked in Fig. 2 *A* with large dots. One such sample with composition of SPM/DOPC/Chol (in molar ratio): 0.30:0.63:0.07 (designated as L_d[lc]) is seen to be just at the edge of the L_d phase. The 11 other samples are seen to have a range of compositions that lie along the edge of the L_o phase. Trial tie-lines were drawn between the L_d[lc] phase composition and each of the L_o compositions as shown by (*solid* or *dashed*) lines in Fig. 2 *A*. Then samples containing 16PC with compositions lying along each of the 11 trial tie-lines were prepared, with 5 samples for each trial tie-line. The compositions along one such tie-line are marked by diamonds in Fig. 2 *A* to illustrate this.

The ESR spectra of all these samples were taken at 22°C, and the method of Chiang et al. (25) was employed to estimate the correct tie-line (i.e., the best of the 11 trial ones). This method utilizes the thermodynamic facts that 1) at any point along the true tie-line the relative amounts of the two coexisting phases (L_o and L_d in this study) is given by the lever rule; and 2) the partition coefficient, K_p, of a probe (16PC in this case) is constant along the true tie-line. Thus, for each trial tie-line, each of the five spectra in the two-component region were fit to the best linear combination of the PB spectra from each end of the tie-line, using the relative populations P measured for the two spectral components, $P(L_d)$ and $P(L_o)$ [with $P(L_d) + P(L_o) = 1$] for each point along the trial tie-line. However, the lever rule applies to the relative amounts of the L_o and L_d phases, and these can be related to the $P(L_d)$ and $P(L_o)$ using the partition coefficient, K_p. That is (25)

$$\frac{[\text{mol\% of } L_d]}{[\text{mol\% of } L_o]} = K_p \frac{P(L_d)}{P(L_o)} = K_p \frac{P(L_d)}{1 - P(L_d)}. \quad (1)$$

Here K_p is the ratio of spin labels partitioning into the L_o phase to those partitioning into the L_d phase when both phases are present in equimolar amounts.

The statistical analysis for fitting the spectra from all five points along the *i*th trial tie-line leads to an estimate of the reduced χ_i^2 (or $\langle \chi_{\text{red}}^2 \rangle_i$) and the estimated K_p (or $\langle K_p \rangle_i$) with standard deviation $\langle \sigma_{Kp} \rangle_i$ (25). The optimal estimate to the true tie-line, as shown by Chiang et al. (25), is a minimum of the product $\langle \chi_{\text{red}}^2 \rangle_i \times \langle \sigma_{Kp} \rangle_i \equiv (\chi^2)_i$. This statistic simultaneously measures the degree to which the linear combination spectra fit to the lever rule and the degree to which K_p remains constant along the trial tie-line. The best estimate to the correct tie-line by this criterion was found to connect the 0.30:0.63:0.07 (L_d[lc]) phase point with the 0.24:0.42:0.34 (designated L_o[mc]) phase point (i.e., the solid tie-line in Fig. 2 *A* marked by *diamonds*). A very recent theoretical study of the phase-diagram for a related model

where there is a possible critical point. The dashed section of the PB to the lower right indicates a region of estimated transition between L_o and L_d phases. The large dots along the PB (1 in L_d phase and 11 in L_o phase) are the compositions at the endpoints of the trial tie-lines and the compositions from which PB spectra were obtained. The solid line with diamonds is the trial tie-line that was determined to be the best estimate to the true tie-line by the method of Chiang et al. (25); this line connects the L_d phase with a mol fraction composition of 0.30:0.63:0.07 (Sm/DOPC/Chol) to the L_o phase with composition 0.24:0.42:0.34 (see respective ESR spectra in Fig. 2 *B*). The five diamonds give the compositions on that tie-line whose spectra (spectra 2–6 in Fig. 2 *C*) were fit by a linear combination of the L_d and L_o PB spectra from the end of the tie-line. The other dashed lines are the 10 other trial tie-lines. (*B*) Demonstrates the differences in the ESR spectra of 16PC at these two boundaries (spectra normalized to a common integrated intensity): dotted line is for L_o, dashed line is for L_d. (*C*) The solid spectra shown and labeled 2–6 are obtained in the two-phase L_o and L_d coexistence region along the tie-line connecting the two boundary spectra, which are again shown as a dotted line for L_o and a dashed line for L_d. Superimposed on the solid spectra 2–6 are dash-dotted ones that represent the appropriate linear combination of L_o and L_d boundary spectra in accordance with the lever rule (25) as the compositions are gradually changed from 100% L_o to 100% L_d (from *top* to *bottom*), as given by the diamonds along the true tie-line shown in Fig. 2 *A*.
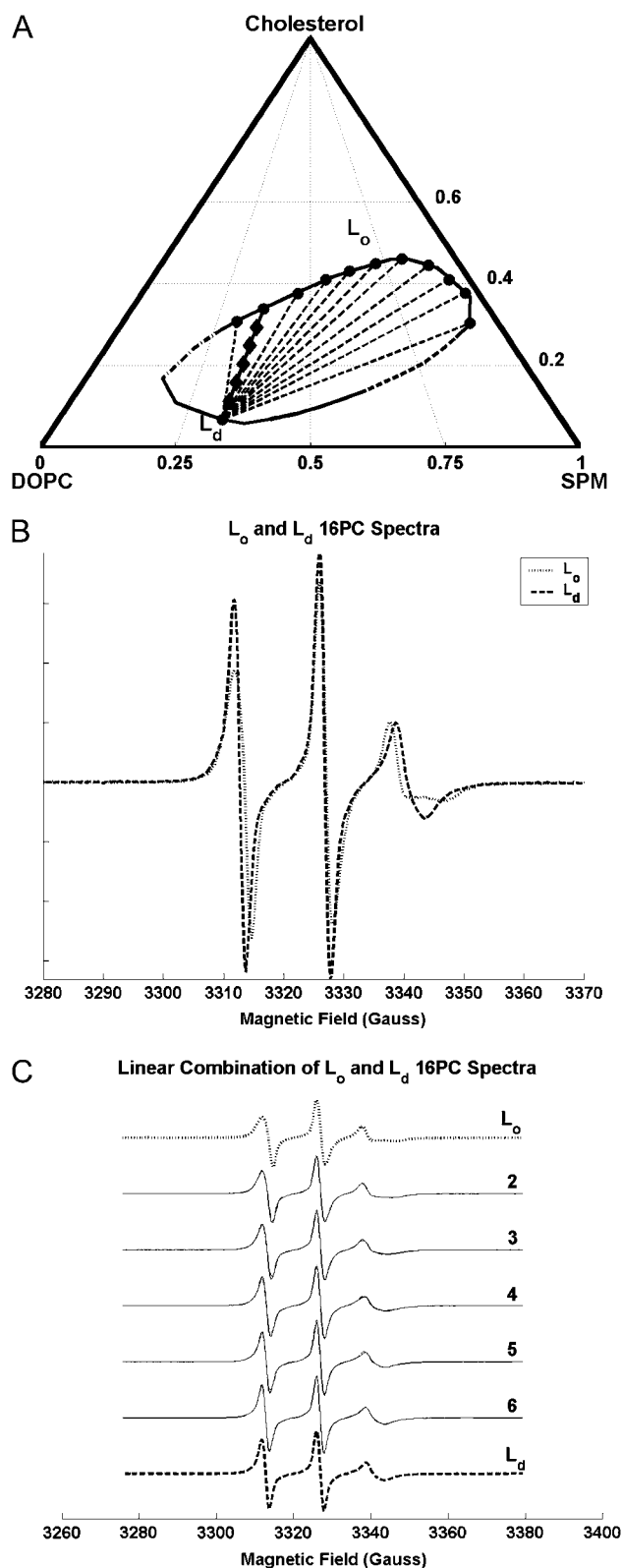
FIGURE 2 Demonstration of tie-line for SPM/DOPC/Chol. (*A*) The ternary (compositional) phase diagram of SPM/DOPC/Chol lipid mixtures at 22°C (22). It contains an elliptical region of coexisting liquid-ordered (L_o) and liquid-disordered (L_d) phases enclosed by a PB (the *elliptical solid line*). The short dotted-dashed section at the far left of the PB indicates roughly

system obtains tie-lines in the L_o-L_d coexistence region that are very similar to the one shown in Fig. 2 *A* (65).

For this method for determining tie-lines to be useful, it is important that the experimental boundary spectra that locate the endpoints of the tie-lines be substantially different. This is the case, as is illustrated in Fig. 2 *B* for the determined tie-line. We show in Fig. 2 *C* how well the ESR spectra along this tie-line are fit by linear combinations of the two ESR spectra at the boundaries. The fits are deemed very good especially in view of experimental uncertainties, such as 1), precise determination of the tie-line, given just a finite number of tentative tie-lines considered; and 2), limits of precision in composition of the prepared samples.

Next, samples of 5, 7, 10, 12, and 14PC with compositions lying along this tie-line, including two at the PB points and five within the coexistence region (as shown by the *diamonds* in Fig. 2 *A*), were prepared and their ESR spectra were taken. Using the L_o and L_d PB spectra as the basis spectra, each spectrum from samples in the two-phase region were fitted to a linear combination of the basis spectra, where the partition coefficient K_p is now the only fitting parameter (25). From these results the mean K_p was determined for each spin label.

Nonlinear least squares analysis of ESR spectra

The ESR spectra were analyzed by a nonlinear least squares (NLLS) method, based on the stochastic Liouville equation (26,27), using the latest version of the ESR fitting program (28). For our evaluation three significant parameters (14) were obtained from the NLLS analysis: 1) $R_\perp$ is the rotational diffusion coefficient of the nitroxide radical around the axis perpendicular to the mean symmetry axis for rotation, which is also taken as the direction of preferential orientation of the spin-labeled lipid molecule. For these spin-labeled PCs the NLLS analysis is found to be insensitive to the $R_\parallel$, the rotational diffusion coefficient of the nitroxide radical around the axis parallel to the mean symmetric axis for rotation, because $R_\parallel$ is typically much greater than $R_\perp$ (14,29). 2) S_0 is the order parameter which is a measure of the angular extent of the rotational diffusion of the nitroxide moiety relative to the membrane normal. 3) P is the relative population of each spectral component in the two-component fits for the cell samples. The average errors estimated for those parameters in the simulation of spectra from live cells are $\pm10\%$ for $R_\perp$, ±0.05 for S_0, and ±0.06 for P; these are slightly larger than the errors in our previous simulations of spectra from PMVs of RBL-2H3 cells (14) because of the lower signal/noise ratios for the spectra from the live cells. The hyperfine tensors and g-tensor values used in the NLLS analysis were taken from those obtained from previous fitting of the rigid limit spectra from the PMVs of RBL-2H3 cells (14), but small variations were allowed in their respective values, consistent with their experimental uncertainties (i.e., $\pm3 \times 10^{-4}$ for g-tensor components and ±0.5 G for hyperfine tensor components).

Kinetics of spin-label quenching

Cells were labeled with different spin-labeled PC analogs essentially as described above except that the centrifugation steps were of 1 min duration. This reduced the time from the addition of spin label to the initiation of spectral recording to $\sim$12–15 min. The time-dependent changes in the intensity of the ESR signal from spin-labeled phospholipids incorporated into the plasma membrane of live RBL-2H3 cells were monitored by setting the magnetic field of the spectrometer on the peak of the midfield line of the ESR spectrum of the nitroxide spin label and keeping the spectrometer in the "timescan" mode, i.e., keeping the field sweep to zero. A modulation amplitude of 5G was used to broaden the peak purposefully to minimize the effect of drift or line width changes during the course of the measurement.

RESULTS

ESR measurements with RBL-2H3, CHO, NIH-3T3, and COS7 cells

Detailed information on the dynamic structure of plasma membranes of live RBL-2H3, CHO, COS7, and NIH-3T3

cells was obtained from NLLS analysis of ESR spectra of the spin-labeled lipids in those cells. The spectra of different spin labels incorporated into the plasma membranes of RBL-2H3 mast cells, recorded at 5°C and 37°C, are shown in Fig. 3 *A* as solid lines. The best fit simulations obtained from this analysis are shown as dashed lines superimposed on the experimental spectra in Fig. 3 *A*. It is seen that the simulated spectra are in very good agreement with the experimental spectra. Fits of comparable quality were also achieved for the spectra from the other cell lines (cf. Fig. 3 *B*).

The spectra of all the spin labels (except for 16PC at higher temperatures) for the RBL-2H3, CHO, COS7, and NIH-3T3 cells required two components for a satisfactory fit. This is shown in the upper spectra in Fig. 3 *B*, where enlarged insets are marked by arrows that point to distinctive features of each of the two components in the spectra of 7PC
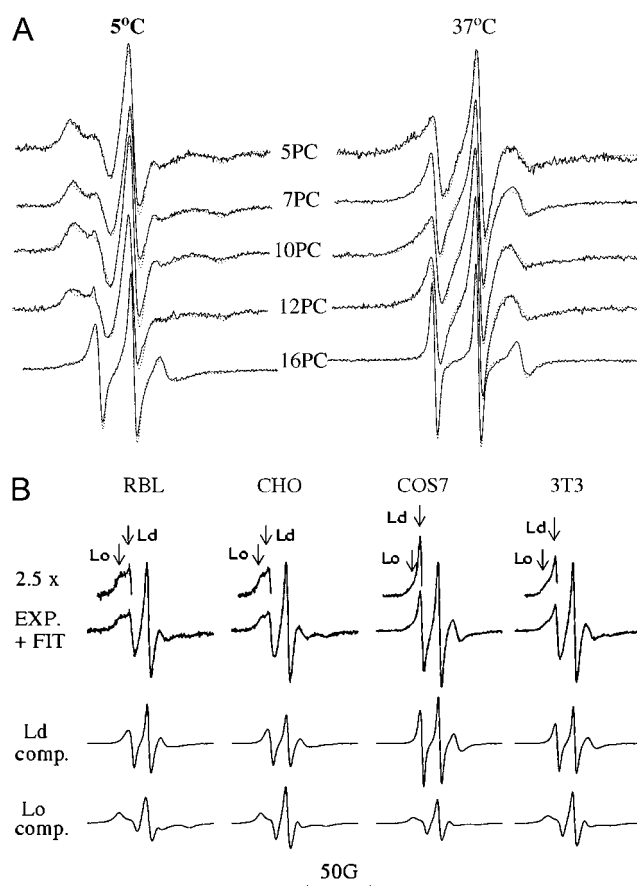

FIGURE 3 ESR spectra of spin labels incorporated into the plasma membrane of live RBL-2H3 mast cells and spectral analysis by the NLLS method. (*A*) Spectra for 5PC, 7PC, 10PC, 12PC, and 16PC in RBL-2H3 cells recorded at 5°C and 37°C (*solid lines*) with the corresponding best fit simulations (*dotted lines*). (*B*) Spectra for 7PC at 25°C in RBL-2H3, CHO, COS-7, and NIH-3T3 cells. Upper spectra show experimental spectra and fits; middle and lower spectra show the resolved spectra for the more mobile (L_d) and less mobile (L_o) components, respectively. The insets to the upper spectra ($\times2.5$ magnification) show distinctive features of both the L_o and L_d components as marked by vertical arrows.
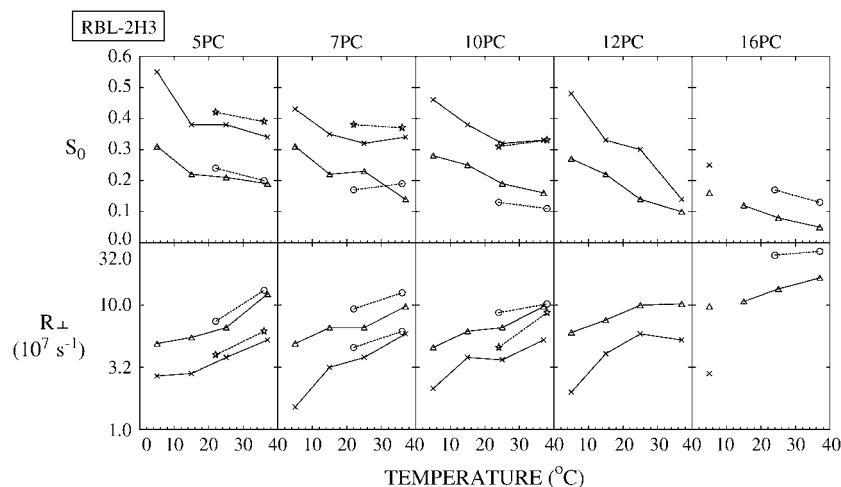
FIGURE 4 For RBL-2H3 cells, the best fit values of the order parameter, S_0, and the rotational diffusion coefficient, $R_\perp$, of the two components (*cross*, L_o component; *triangle*, L_d component) of ESR spectra from different spin labels are plotted versus temperature as solid lines. Also shown are the best fit values of S_0 and $R_\perp$ of the two components (*circle*, L_d component; *star*, L_o component) of ESR spectra from PMV of RBL-2H3 cells (14) plotted versus temperature as dashed lines. The thermally averaged fractions of the L_d spectral component for the live cells $P(L_d)$ are 0.26 ± 0.08 (5PC), 0.26 ± 0.04 (7PC), 0.30 ± 0.03 (10PC), and 0.37 ± 0.10 (12PC).

in the four types of cells at 25°C. Examples of the two spectral components resolved from the fitting are also shown in Fig. 3 B. These two resolved spectral components for each cell type are clearly different, implying that the spin-labeled lipids incorporated into the plasma membrane are found in two regions of the membrane that differ substantially in their dynamic order. A comparison of these two components for the different cell types shows them to be quite similar, implying similar regions within the different plasma membranes. It was shown previously that two-component fits are required for PMV from RBL-2H3 cells (14). Based on the previous studies (13,14) as well as the further analysis described below, we distinguish a more mobile component, which is liquid-disordered (L_d), and a less mobile one, which is liquid-ordered (L_o). The best fit values for the rotational diffusion coefficient, $R_\perp$, the order parameter, S_0, and the relative populations, P, of the two components (i.e., $P(L_d)$ and $P(L_o)$) for 5, 7, 10, 12, and 16PC at various temperatures are presented in Figs. 4–7. The detailed results are provided in Tables S1–S5 (Supplementary Material). Within the fluctuations in the values of $P(L_d)$ with temperature, there

were no discernible trends, so they were simply averaged over temperature to obtain better overall estimates. These averaged values of $P(L_d)$ are given in the figure captions and used in the subsequent discussion.

As shown in Figs. 4–7 for RBL-2H3, COS7, NIH-3T3, and CHO cells, respectively, S_0 for each component generally decreases with increasing temperature, and $R_\perp$ generally increases with temperature, as expected. The results previously obtained from NLLS fits of spectra from spin labels 5, 7, 10, and 16PC in PMVs of RBL-2H3 cells at several temperatures (14) are also plotted in Fig. 4 (*dashed lines*) to compare with the corresponding data from live RBL-2H3 cells (*solid lines*). Clearly, the two sets of results are quite similar, including both the magnitude and temperature variation of the motional rate (measured by $R_\perp$) and the ordering (measured by S_0).

Previously (14) we showed that the more ordered spectral components in the PMV have values of $R_\perp$ and S_0 that are intermediate between that of an L_o phase found in a typical model membrane (e.g., dipalmitoylphosphatidylcholine (DPPC)/Chol = 1:1) or in detergent-resistant membranes
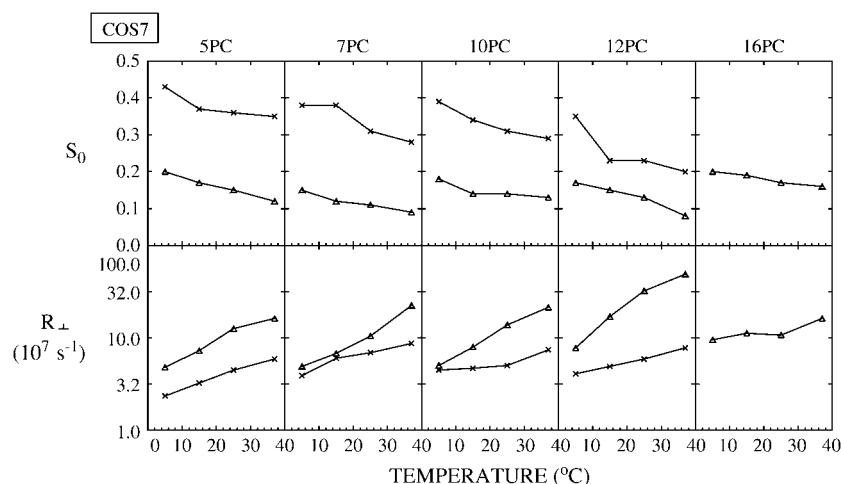

FIGURE 5 For COS7 cells, plots of best fit values of the order parameter, S_0, and the rotational diffusion coefficient, $R_\perp$, of the two components (*cross*, L_o component; *triangle*, L_d component) of ESR spectra from different spin labels versus temperature. The thermally averaged fractions of the L_d spectral component $P(L_d)$ are 0.26 ± 0.04 (5PC), 0.46 ± 0.05 (7PC), 0.42 ± 0.11 (10PC), and 0.45 ± 0.06 (12PC).
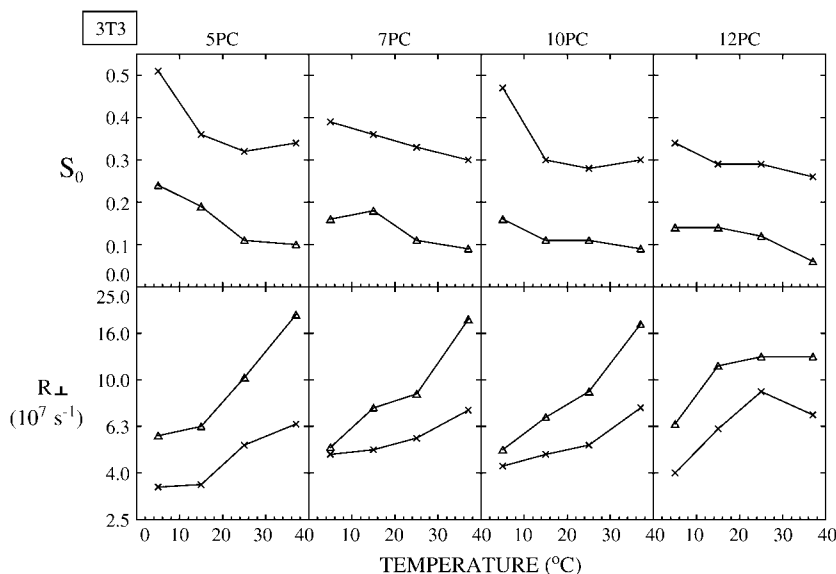
FIGURE 6 For NIH-3T3 cells, plots of best fit values of the order parameter, S_0, and the rotational diffusion coefficient, $R_\perp$, of the two components (*cross*, L_o component; *triangle*, L_d component) of ESR spectra from different spin labels versus temperature. The thermally averaged fractions of the L_d spectral component $P(L_d)$ are 0.37 ± 0.05 (5PC), 0.40 ± 0.12 (7PC), 0.47 ± 0.03 (10PC), and 0.45 ± 0.12 (12PC).

from RBL cells (cf. Ge et al. (13)) and that of an L_d phase as found in pure lipids (13,14). Moreover, $R_\perp$ for the spin labels in the more ordered phase of the PMV are comparable to those in an L_o phase. Thus we characterized the more ordered phase as an L_o phase (referred to in Ge et al. (14) as L_o-like). For the less ordered component we found that its S_0 is substantially less than, and its $R_\perp$ is greater than, those parameters in the L_d phase of pure lipid. Thus it is appropriate to refer to this less ordered phase as an L_d phase. These previous results provided strong evidence for coexistence of L_o and L_d regions in the PMV (14). Thus, the strong similarities in $R_\perp$ and S_0 we have found in this study (cf. Fig. 4) for the two spectral components from the plasma membranes of the live RBL cells and those from the PMV,

prepared from RBL cells, show that L_o and L_d regions also coexist in the plasma membranes of live RBL-2H3 cells. Furthermore, values of $R_\perp$ and S_0 of the two components found for COS7, NIH-3T3, and CHO cells and their temperature variations (Figs. 5–7) are similar to those shown in Fig. 4 for RBL-2H3 cells (also see Tables S1–S4). These results indicate that plasma membranes for all four cell types have similar coexisting L_o and L_d regions.

We observe that $P(L_d)$ for the PMV from RBL-2H3 cells is consistently lower than for the live RBL-2H3 cells. Thermally averaged values of these $P(L_d)$ are 0.11 vs. 0.26 for 5PC, 0.11 vs. 0.26 for 7PC, and 0.19 vs. 0.30 for 10PC. (cf. Table 1 in Ge et al. (14) and Table S1 in Supplementary Material for this work).
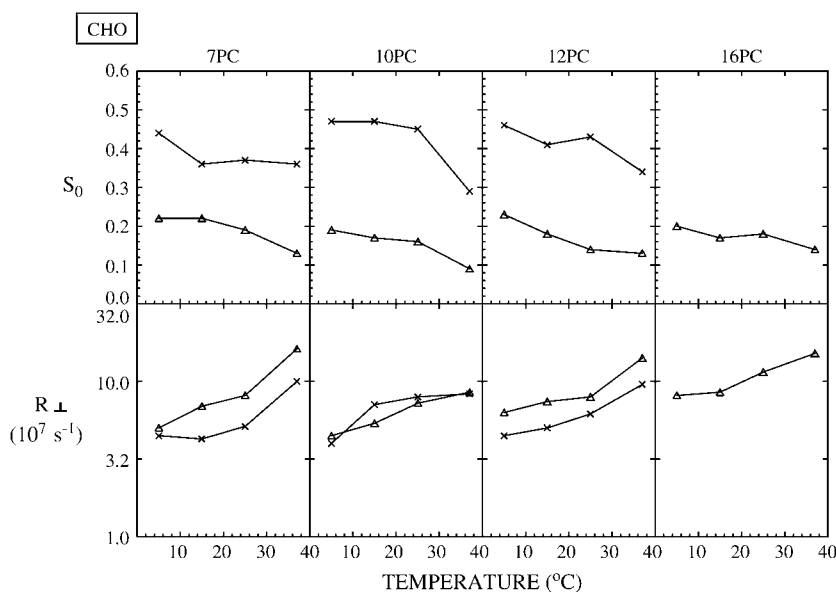

FIGURE 7 For CHO cells, plots of best fit values of the order parameter, S_0, and the rotational diffusion coefficient, $R_\perp$, of the two components (*cross*, L_o component; *triangle*, L_d component) of ESR spectra from different spin labels versus temperature. The thermally averaged fractions of the L_d spectral component $P(L_d)$ are 0.25 ± 0.10 (7PC), 0.38 ± 0.02 (10PC), and 0.41 ± 0.11 (12PC). Because of the low signal/noise ratio of the spectra from 5PC in CHO cells, we could not get a good fit for this case; so these results are not provided.
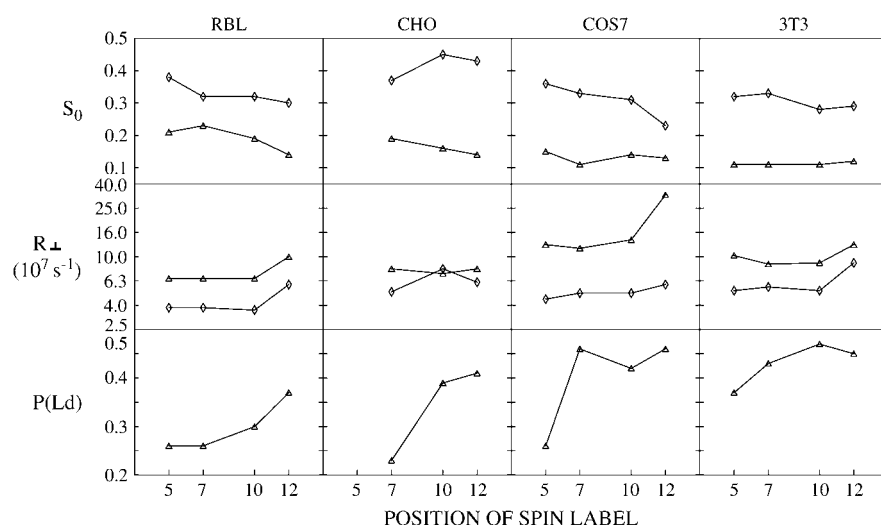
FIGURE 8 Plots of best fit values of the order parameter, S_0, the rotational diffusion coefficient, $R_\perp$, of the two components at 25°C (*diamond*, L_o component, *triangle*, L_d component) and (thermally averaged) fraction of the L_d component, $P(L_d)$ of ESR spectra from spin labels 5, 7, 10, and 12PC in RBL-2H3, CHO, COS7, and NIH-3T3 cells, versus the position of nitroxide radical attached at the acyl chain.

To assess accurately the relative amounts of the two types of regions in the live cells, from the respective measured values of P, the partition coefficient K_p of the spin-labeled lipid is needed (cf. Eq. 1). Although it is not possible to measure directly the K_p for the PC labels in live cells, a method exists for obtaining these values in model membranes with coexisting phases (25) as described in the Materials and Methods section. Previous estimates were based on a lipid mixture showing coexistence between liquid-crystalline and gel phases (14,25). The SPM/DOPC/Chol 3-component system exhibits a region of coexistence between L_o and L_d phases (cf. Fig. 2 *A* and 22–24), providing a more appropriate model system from which to obtain the estimated K_p. Using the method of Chiang et al. (25), described in the Materials and Methods section, we estimated values of K_p of 0.4 ± 0.2, 0.5 ± 0.2, 0.6 ± 0.2, 0.6 ± 0.2, 0.8 ± 0.4, and 1.1 ± 0.5 for 5, 7, 10, 12, 14, and 16PC, respectively. $K_p = 1$ corresponds to equal partitioning in the L_o and L_d phases, and K_p less than unity means the L_d phase is preferred (cf. Eq. 1). Thus this model system shows that all the spin-labeled PCs partition into both the L_o and L_d phases, and the PCs labeled farther up the chain have a moderate preference for the L_d phase. If these K_p results for 5PC through 12PC ($K_p \sim 0.5$) are used as a rough estimate in Eq. 1 for the RBL-2H3 cells and if the measured $P(L_d)$ for the spin probes in these cells (in the range of 0.2–0.4, see caption to Fig. 4 and Table S1) are also inserted into Eq. 1, then Eq. 1 indicates that the L_o component is the major component in the plasma membranes of RBL-2H3 cells. The results for the other three cell lines (cf. captions to Figs. 5–7 and Tables S2–S4) are also consistent with a major L_o component.

Some comments apply to the results for 16PC shown for RBL-2H3, COS7, and CHO cells in Figs. 4, 5, and 7 (because the 16PC spectra in NIH-3T3 cells decay rapidly, they are too noisy to be analyzed). Only a single component is observed, except for the 5°C result for RBL-2H3 cells in Fig. 4. In this case the single component at higher tem-

perature appears to be consistent with a continuation of the L_d phase. However, for the other two cell lines, and in general, it is difficult to discern whether the 16PC is in the L_d or L_o phase or whether the values obtained represent some average over the two phases.

Our NLLS analysis revealed some common features and some differences in the dynamic structures among the four cell lines. Plotted in Fig. 8 are variations of $R_\perp$ and S_0 of the two components, and the thermally averaged $P(L_d)$ with respect to the position of nitroxide radical attached to the acyl chain at 25°C for the four cell lines. From Fig. 8 we can see the following similarities: 1) The profiles of S_0 versus position of the label for both the L_o and L_d regions tend to be fairly flat; 2) $R_\perp$ tends to be flat from C5 to C10 followed by an increase at C12; and 3) $P(L_d)$ increases as the nitroxide moiety is placed farther down the acyl chain. This suggests that PCs labeled farther down the chain partition more favorably into a disordered plasma membrane environment, a matter we discuss further below.

The experimental spectra and their analyses do illustrate further similarities as well as differences among the different cell lines. The experimental 7PC spectra and the two components extracted by our NLLS analysis from these spectra for the four types of cells at 25°C are shown in Fig. 3 *B*. It is seen that whereas they are similar, there are significant differences between the RBL-2H3 and CHO cells, on the one hand, and the NIH-3T3 and COS-7 cells, on the other. More precisely, we note the L_o spectral component for the four cell lines are similar, but the L_d spectral component of COS7 and NIH-3T3 cells is narrower than that of RBL-2H3 and CHO cells. Such differences are also seen between the spectral components for the four cell types at temperatures of 5°C and 15°C (data not shown). The source of the spectral differences is readily explained by the results in Fig. 8 and in Tables S1–S4. That is, 1) the rotational diffusion coefficients $R_\perp$ for the L_d component of the COS7 cells (3.75 × 10⁷–2.26 × 10⁸ s⁻¹) and the NIH-3T3 cells (4.79 × 10⁷–1.82 × 10⁸ s⁻¹) are

slightly higher than those for the L_d component of the RBL-2H3 cells (1.52×10^7–9.97×10^7 s^{-1}) and CHO cells (4.50×10^7–1.61×10^8 s^{-1}); and 2) the order parameters, S_0, are lower in the COS7 (0.09–0.15) and NIH-3T3 cells (0.09–0.16) than in RBL-2H3 (0.14–0.31) and CHO cells (0.13–0.22). In summary, the L_d region for the COS7 and NIH-3T3 cells shows slightly greater 'fluidity' than that for the other two cell lines. Furthermore, 3) the $P(L_d)$ for COS7 and NIH-3T3 cells is larger than those for RBL-2H3 and CHO cells (Fig. 8).

14PC and 16PC in the live cells exhibit rather different behavior as compared with the other spin-labeled PCs (5, 7, 10, and 12PC). The ESR spectra of 14PC and 16PC in all four types of cells exhibit substantial broadening (except for the 16PC spectra in RBL-2H3 cells). Fig. 9 shows some examples. The analysis of the 16PC spectra from COS7 and CHO yields two components: one sharp and well resolved, and one very broad. The values shown in Table S5 and Figs. 5 and 7 correspond to the sharp component, and Table S5 provides its relative population. The second component is a single broad line, indicative of strong spin-spin interactions due to clustering of the 16PC spin labels (30,31). These spectra, containing a broad and a sharp component, are similar to those from 16PC in detergent-resistant membranes derived from RBL-2H3 cells (13). All the spectra from 14PC in the cells exhibited characteristics similar to those from 16PC (Fig. 9). However, unlike the other spin-labeled PCs, the 14PC spectra were not reproducible with different cell culture preparations, so that a detailed analysis was not useful.

ESR measurements with model membranes

The SPM/DOPC/Chol ternary system, which shows coexistence of L_o and L_d phases, has been used as a model membrane

to mimic the structure of biological membranes, and phase diagrams have been constructed (cf. Fig. 2 A and 22–24). As described above we used this system to obtain estimates of K_p, and we also consider it appropriate for purposes of comparison with our results from plasma membranes of live cells. This is because 1) this lipid system is considered to be representative of the lipid content of biological membranes (22–24,32); and 2) it exhibits a coexistence region for the L_o and L_d phases, which is clearly relevant to the results on the live cells, as we have noted above. Also, we have obtained for this system the extensive results from spin labels covering the full range of positions along the acyl chain.

Thus, ESR spectra of 5, 7, 10, 12, 14, and 16PC in vesicle dispersions of SPM/DOPC/Chol at 22°C were analyzed. We used three different compositions of SPM/DOPC/Chol with molar ratios of 0.43:0.11:0.46 (L_o[hc]), 0.24:0.42:0.34 (L_o[mc]), and 0.30:0.63:0.07 (L_d[lc]). The designations [hc], [mc], and [lc] correspond to high, moderate, and low concentrations of cholesterol. The first two yield L_o phases that are at the PB with the two-component L_o-L_d region. The third yields an L_d phase also at the PB. Estimates of tie-lines (cf. Materials and Methods section and (25)) indicate that L_o[mc] and L_d[lc] coexist in the two-phase region (i.e., they are connected by a tie-line), as we have discussed above. The L_o[mc] composition was motivated by the known concentration of cholesterol in the plasma membranes of RBL-2H3 cells, which was measured to be 33 mol % in a previous study (33). More generally, the content of cholesterol in plasma membranes is typically 30–40 mol % (16).

In all these cases, our NLLS analysis showed that the spectra were well fit with just a single component, as expected for these spin-labeled lipids in a single phase. The best fit values of $R_\perp$ and S_0 for these spectra are listed in Table S6 of Supplementary Material. The profiles of $R_\perp$ and S_0 with respect to the position of the acyl chain nitroxide label for the PCs for the three compositions are shown in Fig. 10. The
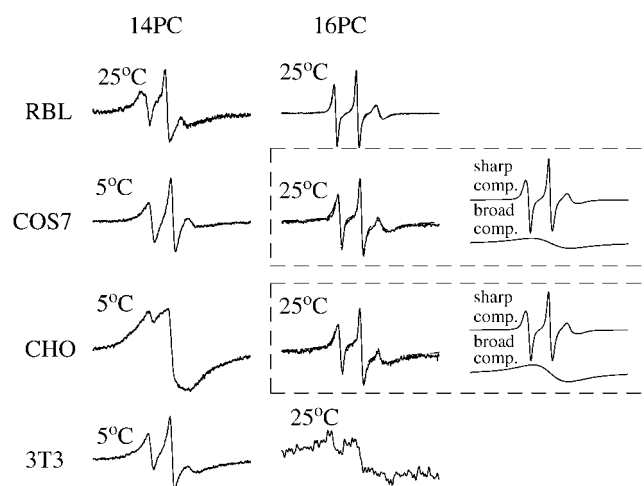
FIGURE 9 ESR spectra of 14PC and 16PC in the plasma membranes of live RBL-2H3, COS7, CHO, and NIH-3T3 cells (experimental, *solid lines*; simulations, *dashed lines*). The temperatures at which these spectra were recorded are indicated at the corner of each spectrum. For illustration, the calculated two components of 16PC spectra in COS7 and CHO cells are shown in the two boxes.

FIGURE 10 Plots of best fit values of the order parameters, S_0, and the rotational diffusion coefficient, $R_\perp$, of ESR spectra from spin labels 5, 7, 10, 12, and 16PC in lipid dispersions of SPM/DOPC/Chol with three different compositions (see text) at 22°C versus the position of nitroxide radical attached at the acyl chain, solid lines. Relevant results for RBL-2H3 cells at 25°C from Fig. 8 are shown by dashed lines for comparison.

profiles look similar in that $R_\perp$ increases substantially from 5PC to 16PC, whereas S_0 decreases over this range of positions of the spin label.

This negative slope of S_0 is, however, seen to increase with decreasing cholesterol concentration. That is S_0 for 5PC is comparable for all three compositions, but for 16PC it is much smaller for L_d[lc] than for the two L_o phases. This is consistent with the packing of the acyl chain near the headgroup region being comparably tight for the three compositions, but it becomes less constrained with decreasing cholesterol near the center of the bilayer. The positive slope of $R_\perp$ is seen to decrease with decreasing cholesterol concentration. That is, $R_\perp$ for 5PC is largest for L_d[lc] and smaller for L_o[mc] and L_o[hc]. But they are more nearly comparable near the center of the bilayer. This indicates that the local friction, which has a major role in determining $R_\perp$, is comparable in the three cases near the center of the bilayer but does vary with cholesterol near the headgroup, being least for L_d[lc] and most for L_o[hc].

It is possible to make a partial comparison of these ESR results on the three-component SPM/DOPC/Chol model membrane system with those from the DLPC/DPPC/Chol model membrane that was previously studied at 24°C in these laboratories (34). This latter study was more extensive in one sense—it covered most of the phase diagram—but less extensive in that 16PC was the only spin-labeled lipid used. Despite the very significant differences in phospholipid components and the very different phase diagrams in the two cases (e.g., the latter does not have an L_o-L_d two phase coexistence region), we find some good comparisons in respective values for S_0 and $R_\perp$ for 16PC. Some examples are given in Table 1. The conclusion appears to be that the respective phases for the two different mixed lipid membrane systems have quite similar dynamic molecular properties as viewed by the end-chain label 16PC.

In another limited comparison for the behavior of 16PC in the two different ternary mixtures, we consider the value of K_p. In this work, a value of $K_p = 1.1 \pm 0.5$ was obtained for the coexistence of the L_d[lc] and L_o[mc] compositions. In

previous work on the DLPC/DPPC/Chol system the main two-phase region is L_d and gel; there $K_p = 0.9 \pm 0.1$ was found for the case of 0% Chol, decreasing to 0.6 ± 0.2 for the 13%–15% Chol tie-line (25), where $K_p < 1$ favors the L_d phase. Thus K_p values of roughly comparable magnitude are obtained for the L_d-L_o and L_d-gel coexistence regions for 16PC.

Comparison of results on live cells with those from model membranes

To directly compare the results on live cells with those from the model membranes at 22°C we also show by dashed lines in Fig. 10 the profiles of S_0 and $R_\perp$ of both the L_o and L_d components for the RBL-2H3 cells at 25°C given in Fig. 8. The profiles of $R_\perp$ for the L_o and L_d phases of the live cells are very similar to those of the L_o[mc] and L_d[lc] phases, respectively, of the model membrane, indicating similar mobilities in these respective membrane phases. Also, the profiles of S_0 in the L_o and L_d phases of the RBL-2H3 cells are comparable to those for the respective model membrane phases, although the live cell results do show less variation along the acyl chain. It is shown in Fig. 8 that the profiles of S_0 and $R_\perp$ for the four cell lines are similar, so it follows that they are all similar to those of the model membranes.

Such similarities between the respective coexisting L_o and L_d phases for the live cells and the model membranes for the range from 5PC to 12PC are intriguing given the large differences in their lipid compositions and the absence of proteins in the model membranes. This also provides the best argument for using the K_p values observed for the 5–12PC spin labels in the model membrane as a rough guide for the live cell plasma membranes.

The end-chain spin labels reveal some differences. In particular, that 14PC and 16PC in the live cells tend to cluster (cf. Fig. 9) is clearly different behavior from what is observed in model membranes consisting of pure or mixed lipid systems. It is possible that these spin labels are not being fully incorporated into the cell plasma membrane. However, this does not seem to be the most likely explanation, because the other spin-labeled lipids (nPC, $n = 5$, 7, 10, 12) are readily incorporated and do not show such behavior. In fact, in our extensive experience with 14PC and 16PC in model membranes and PMV we find they are readily incorporated into the membrane phase (13,14,25,29, 31,34–37). Clearly the presence of membrane proteins in the plasma membranes of live cells is a major difference from the model membranes. Previous studies have shown that reconstitution of integral membrane proteins into lipid bilayers dramatically increases the water permeability (38); incorporation of a small peptide into PC bilayers also increases water penetration (39), and this suppresses the polarity gradient of the membrane (31). On the other hand, cholesterol, such as is present in an L_o phase, reduces the water penetration into lipid bilayers (40). One possibility,

TABLE 1 Some comparisons of S_0 and $R_\perp$ for 16PC in the model membrane systems DLPC/DPPC/Chol and SPM/DOPC/Chol

Composition and phase		S_0	$R_\perp$
Phase DLPC/DPPC/Chol*[†]	Phase SPM/DOPC/Chol[‡]		$(10^8 s^{-1})$
L_d 0.48/0.32/0.20		0.13	1.8
	L_d [lc]/0.30/0.63/0.07	0.09	2.1
L_o 0.56/0.14/0.30		0.22	2.2
	L_o [mc]/0.24/0.42/0.34	0.20	2.2
L_o 0.24/0.24/0.52		0.26	2.3
	L_o [hc]/0.43/0.11/0.46	0.27	3.8

*24°C.

[†]From Chiang et al. (34). The results on 16PC (34) for the DLPC/DPP/Chol system show only slight to modest variation in S_0 and $R_\perp$ versus composition within a respective phase.

[‡]22°C.

suggested by these observations, is a more substantial presence of water molecules in the L_d phase of cell membranes, especially near the center of the bilayers, where the acyl chain segments are more loosely packed. Such regions of higher polarity could accumulate 14PC and 16PC because their polar nitroxide group is better accommodated. This scenario might help explain the somewhat greater preference of 10PC and 12PC for the L_d region of live cells as compared to 5PC and 7PC (cf. the $P(L_d)$ shown in Fig. 8).

Kinetics of ESR signal decay

During the ESR measurements of spin-labeled live cells, the ESR signal intensity was observed to decay with time. Lowering the temperature reduced the signal decay, but even at 5°C the decay was detectable. We examined the kinetics of this process by measuring the intensity of the central peak of the ESR spectra of different PC spin labels incorporated into the plasma membrane of RBL-2H3 cells as a function of time at 5, 15, and 22°C. The ESR signal intensities of different spin labels viz., 5PC, 10PC, and 12PC, monitored as a function of time at 5°C are shown in Fig. 11.

All the kinetic traces obtained at 5°C could be fit to a monoexponential decay (shown as an overlapping *white line* on each kinetic trace). At this low temperature internalization of the plasma membrane lipids due to endocytosis is insignificant. Therefore, any decay in the ESR signal is most likely due to the reduction of the nitroxide moiety by the free thiol groups of membrane-associated proteins (41). In separate experiments we used fluorescence quenching to compare the location of 10PC with BODIPY-GM1, which is observed with fluorescence microscopy to be retained in the plasma membrane of RBL-2H3 cells. The results showed that most of the 10PC stays in the plasma membrane together with the BODIPY-GM1 for at least an hour (Fig. S1 in Supplemental Materials).

At higher temperatures (15 and 22°C), the decay process becomes more complex and the decay profiles could not be fit to monoexponential functions (not shown). This is most likely due to the fact that at these temperatures and time periods, the signal may decay by reduction in the intracellular milieu upon endocytosis of the spin-labeled probes from the plasma membrane, in addition to reduction of the nitroxide moiety by the membrane surface thiols.

Constancy of ESR spectra as a function of time

During the course of our ESR experiments we have performed extensive tests of the constancy of the ESR spectra as a function of time. We present one such example in Fig. 12. From this figure, it can be seen that the ESR spectra of 7PC recorded successively at 30°C are virtually identical in shape although the actual spectral intensity has decreased with time. This is reflected in the significantly lower S/N ratio for spectrum 2 as compared to spectrum 1. All similar tests we have performed demonstrate that the spectra from the cell plasma membranes remain constant in their line shapes even as they decay in intensity with time.

DISCUSSION

The results show that ESR spectra of chain spin-labeled PCs in the plasma membrane of live RBL-2H3, CHO, COS7, and NIH-3T3 cells consist of two components, which are characteristic of L_o and L_d phases. These components are similar to those in PMVs of RBL-2H3 cells previously described (14), and they provide direct evidence for the L_o-L_d phase separation in the plasma membrane of live cells. We address two matters specific to the results on live cells before discussing the significance of these new findings.
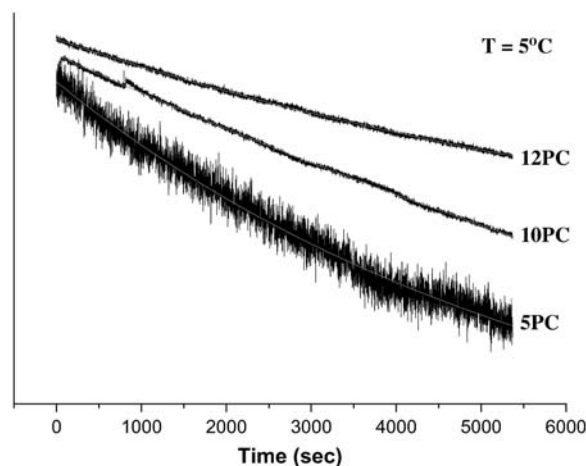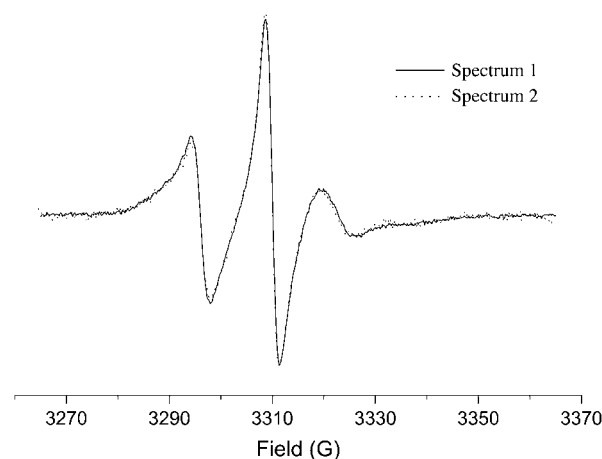

FIGURE 11 Kinetics of ESR signal decay of 5PC, 10PC, and 12PC incorporated into the plasma membranes of RBL-2H3 cells. The intensity of the central ESR line was monitored as a function of time at 5°C.

FIGURE 12 ESR spectra of 7PC in live RBL-2H3 cells at 30°C spectrum 2 (*dotted line*) was recorded after spectrum 1 (*solid line*). Both spectra are the sum of 32 repeated scans each. Accumulation of the scans for spectrum 2 was completed 28 min after spectrum 1 was completed. Spectrum 2 was vertically expanded to match spectrum 1 for the purpose of comparison.

The two spectral components are not generated by internalization of spin labels

We considered the possibility that the two different environments, yielding L_o and L_d populations, could be the result either of internalization or of flip-flop of a fraction of the spin label. If this happens significantly, then one of the spectral components could be due to the spin label in the outer leaflet of the plasma membrane and the second component could be due to the spin label that is internalized or located in the inner leaflet. However, the following observations clearly indicate that such a possibility is highly unlikely. 1) The flip-flop of the spin label from the outer leaflet of the plasma membrane into the inner leaflet is expected to be negligible during the course of the experiment (~1 h), because the flip-flop rates of PC in different systems have been shown to be very low in most cases (42,43). 2) The ESR spectra obtained from the same sample from repeated accumulations remain nearly identical in line shape (Fig. 12), suggesting that the lipid environment of the detectable spin labels is not altered during this time period. 3) We performed kinetic measurements at different temperatures. They show that whereas the spectral line shape does not change with time, its intensity decays over a period of 1–3 h even at temperatures as low as 5°C (Fig. 11), where endocytosis is drastically reduced (44) and flip-flop is expected to be negligible (42,43). This decay rate varies substantially with location of the label on the acyl chain: those closer to the headgroup region decay more rapidly (Fig. 11). It is possible that the nitroxide moiety of the spin-labeled PC analogs are being reduced in the plasma membrane by thiol groups of peripheral/integral membrane proteins (41). 4), Fluorescence microscopy shows that, when RBL-2H3 cells are labeled with fluorescently labeled lipid probes such as BODIPY-GM1 at $T \leq 5°C$, the label is retained in the plasma membrane for more than an hour (P. Sengupta, unpublished results). In the double-labeling experiments in which the RBL-2H3 cells were labeled with both BODIPY-GM1 and 10PC, the time-dependent relief of quenching of the fluorescent lipid probe by the phospholipid spin probe as it decays confirms that they both exist in the same region of the RBL-2H3 cells (Fig. S1, Supplementary Material).

The two spectral components are not due to coexistence of boundary and bulk lipids

The concept of boundary lipids was derived from the broad spectral components observed in ESR spectra from acyl chain spin labels, mostly of 14PC and 14-(4′,4′-dimethyl-oxazolidine-N-oxyl) steric acid, in protein/lipid complexes that have been characterized previously. These broad components have large outer peak separations, usually >60 G. The rotational diffusion coefficients of these lipid molecules were estimated to be approaching the rigid limit on the ESR timescale (45), i.e., these lipids are immobilized. It was

suggested that the broad component represents lipid molecules in contact with the protein molecules (35,45–49). This spectral component compares favorably with the boundary lipid component found by Ge and Freed (36) in their study of 16PC in gramicidin A in DPPC, which they pointed out is gel-like (see also Costa-Filho et al. (37)).

In this work on the live cells, the outer peak separation of the L_o component of the 5PC spectra at 25°C is <57 G and that of the spectrum of 12PC in RBL-2H3 cells at 25°C is only 48 G, which is much smaller than 60 G, and its ESR spectrum is clearly different from those of boundary lipid, previously reported (cf. 36,48). As described above, the ESR spectral component from the live cells (and PMV) that is attributed to the L_o phase has many characteristics of ESR spectra from L_o phases in model membranes (see also Ge et al. (13,14) and Costa-Filho et al. (50)), and they are qualitatively different from those of boundary lipids. Thus, we conclude that our ESR observations in the live cells (as well as in the PMV) are not due to boundary lipids.

Live cells versus PMV and model membranes

Transmembrane proteins in plasma membranes have an important effect on the organization and dynamic structure of plasma membranes (5,51). Transmembrane proteins could disturb a fragile ordering of the lipids in their surrounding environment in the plasma membranes, thereby rendering them more disordered and mobile. This may be at least partially responsible for the observation of the L_d phase in the cell plasma membranes. The observation of a larger L_d spectral component in the live RBL-2H3 cells than in the PMV is consistent with the lower protein content in PMV as compared to the plasma membrane of the live RBL-2H3 cells (52). Moreover, it was found that by studying the lipids extracted from the PMV, the L_d component was eliminated leaving only the L_o component in the ESR spectrum (14). (This further argues against assigning the L_o component to boundary lipids.) Also, recent studies with model systems demonstrate that incorporation of transmembrane peptides into membranes with ordered bilayers can result in the formation of disordered regions (53), and this lends further support to the above interpretation. It has even been hypothesized that proteins play a central role in organizing cell membranes into domain structures (5,54). Also, the actin cytoskeleton that attaches to the plasma membrane in cells but not in PMV (55,56) may also play a role in the differences between PMV and live cells. Of further relevance is the fact that the cell maintains active processes of protein and lipid turnover and is not at equilibrium, unlike membrane vesicle preparations.

It is known that liquid-liquid immiscibility in membranes depends on the cholesterol concentration (57,58) and that a substantial concentration of cholesterol in a membrane is crucial for the formation of an L_o phase (13,59,60). Thus, the substantial amounts of cholesterol contained in the live cell

membranes that we have studied, as well as in the SPM/DOPC/Chol model membranes, is a very likely reason the phase structures of the two membrane systems are similar. In a recent review article, London commented that a ternary mixture consisting of a high melting temperature (T_m) lipid (e.g., sphingolipids with saturated acyl chains), a low T_m lipid (e.g., phospholipids with unsaturated acyl chains), and cholesterol may crudely imitate cell membrane behavior (32). The results of this study on just such a model system (SPM/DOPC/Chol), in comparison with the live cell membranes, support this comment.

Thus, the results in this study are consistent with the view that the effect of proteins on the structure of membranes (i.e., lipid/protein interactions) and substantial concentrations of cholesterol (i.e., lipid/lipid interactions) both contribute to domain formation in cell membranes.

Insights into the structure of cell plasma membranes

On the basis of the similar dynamic structural properties of $R_\perp$ and S_0 in the live cells versus the model membrane system that was observed over the range of acyl chain spin labels from 5PC to 12PC, we have concluded (Results section) that the partition coefficients, K_p, measured for the latter should provide a reasonable, albeit rough estimate of the partitioning in the former. Using these K_p values one finds that the L_o component is a major component and quite possibly the predominant component in the plasma membranes of the live cells.

This result contradicts the view of small L_o regions of lipids or "rafts" floating in a larger sea of disordered lipid (1,2,5,6). Instead, this result lends itself more readily to an interpretation in terms of a model of a continuous L_o phase in the outer leaflet of the plasma membrane (16). Such a continuous L_o phase model could include the possibility of small scale dynamic variations of the order of several lipid molecules in size in the L_o regions (51,61) whose effects could be averaged out on the ESR timescale. In fact, a continuous L_o phase was demonstrated in a recent study on a model membrane consisting of brain SPM, brain PC, and cholesterol (60). That is, as the concentration of cholesterol in the model membrane was increased, a point was reached at which the L_o phase (rafts) changed from a disconnected to a connected (or continuous) one. At this percolation point, the cholesterol concentration is 20–30 mol %, and the amount of the L_o (or raft) phase, relative to the L_d phase, is 45%–50% (60). These concentrations are comparable to what we have estimated in this study for the live cells.

With fluorescent probes it is not possible to distinguish L_o and L_d phases on live cell membranes under an optical microscope, indicating that the dimensions of at least one of them must be less than $\sim$300 nm in the absence of receptor cross-linking or other perturbations. The ESR spectra are not able to provide an accurate estimate of the size of the membrane domains but can provide a rough estimate of a lower bound for this dimension. Based on the measured diffusion coefficients for PC spin labels in model membranes (62,63), as well as the fact that the diffusion between the regions is too slow to average the two distinctly different spectral components, one can roughly estimate that their size should be greater than $\sim$2 nm. This estimate of a lower bound on the domain size is consistent with the recently proposed scenario, that in resting cells, rafts appear small; they might be as small as a molecular complex consisting of only three molecules, but their size distribution is broad (56). This is to be compared with the size of domains in model membranes, which has been observed in the range of 80 nm to tens of micrometers, depending on how the model membranes were prepared and which techniques were used to measure domain size (8,60,64).

SUMMARY

The ESR studies reported here demonstrate the presence of two distinct lipid populations with different order parameters and dynamic rate, corresponding to L_o and L_d phases, in the plasma membranes of live cells. These results serve as a baseline for interpreting studies of cellular processes that are related to the phase-like behavior of the plasma membrane. Spin-label ESR spectroscopy, coupled with the NLLS analysis, provides a method that is applicable in the study of the dynamic phase structure of membranes in live cells.

SUPPLEMENTARY MATERIAL

An online supplement to this article can be found by visiting BJ Online at http://www.biophysj.org.

REFERENCES

1. Simons, K., and D. Toomre. 2000. Lipid rafts and signal transduction. *Nat. Rev. Mol. Cell Biol.* 59:950–957.

2. Brown, D. A., and E. London. 1998. Functions of lipid rafts in biological membranes. *Annu. Rev. Cell Dev. Biol.* 14:111–136.

3. Young, R. M., D. Holowka, and B. Baird. 2003. A lipid raft environment enhances Lyn kinase activity by protecting the active site tyrosine from dephosphorylation. *J. Biol. Chem.* 278:20746–20752.

4. Young, R. M., X. Zheng, D. Holowka, and B. Baird. 2005. Reconstitution of regulated phosphorylation of FcεRI by a lipid raft-excluded protein tyrosine phosphatase. *J. Biol. Chem.* 280:1230–1235.

5. Edidin, M. 2003. The state of lipid rafts: from model membranes to cells. *Annu. Rev. Biophys. Biomol. Struct.* 32:257–283.

6. Mukherjee, S., and F. R. Maxfield. 2004. Membrane domains. *Annu. Rev. Cell Dev. Biol.* 20:839–866.

7. De Almeida, R. F., A. Dedorov, and M. Prieto. 2003. Sphingomyelin/phosphatidylcholine/cholesterol phase diagram: boundaries and composition of lipid rafts. *Biophys. J.* 85:2406–2416.

8. Feigenson, G. W., and J. T. Buboltz. 2001. Ternary phase diagram of dipalmitoyl-PC/dilauroyl/cholesterol: nanoscopic domain formation driven by cholesterol. *Biophys. J.* 80:2775–2788.

9. Dietrich, C., L. A. Bagatolli, Z. N. Volovyk, N. L. Thompson, M. Levi, K. Jacobson, and E. Gratton. 2001. Lipid rafts reconstituted in model membranes. *Biophys. J.* 84:725–726.

10. Veatch, S. L., and S. L. Keller. 2003. Separation of lipid phases in giant vesicles of ternary mixtures of phospholipids and cholesterol. *Biophys. J.* 85:3074–3083.

11. Schroeder, R., E. London, and D. Brown. 1994. Interactions between saturated acyl chains confer detergent resistance on lipids and glycosylphosphatidylinositol (GPI)-anchored proteins: GPI-anchored proteins in liposomes and cells show similar behavior. *Proc. Natl. Acad. Sci. USA.* 91:12130–12134.

12. Heerklotz, H. 2002. Triton promotes domain formation in lipid rafts mixtures. *Biophys. J.* 83:2693–2701.

13. Ge, M., K. A. Field, R. Aneja, D. Holowka, B. Baird, and J. H. Freed. 1999. Electron spin resonance characterization of liquid ordered phase of detergent-resistant membranes from RBL-2H3 cells. *Biophys. J.* 77:925–933.

14. Ge, M., A. Gidwani, H. A. Brown, D. Holowka, B. Baird, and J. H. Freed. 2003. Ordered and disordered phases coexist in plasma membrane vesicles of RBL-2H3 mast cells. An ESR study. *Biophys. J.* 85:1278–1288.

15. Holowka, D., J. A. Gosse, A. T. Hammond, X. Han, P. Sengupta, N. L. Smith, A. Wagenknecht-Wiesner, M. Wu, R. M. Young, and B. Baird. 2005. Lipid segregation and IgE receptor signaling: a decade of progress. *Biochim. Biophys. Acta.* 1746:252–259.

16. Munro, S. 2003. Lipid rafts: elusive or illusive? *Cell.* 115:377–388.

17. Pierini, L., D. Holowka, and B. Baird. 1996. Fc(epsilon)RI-mediated association of 6-micron beads with RBL-2H3 mast cells results in exclusion of signaling protein from the forming phagosome and abrogation of normal downstream signaling. *J. Cell Biol.* 134:1427–1439.

18. Field, K. A., D. Holowka, and B. Baird. 1999. Structural aspects of the association of FcepsilonRI with detergent-resistant membranes. *J. Biol. Chem.* 274:17531–17538.

19. Thomas, J. H., D. Holowka, B. Baird, and W. W. Webb. 1994. Large-scale co-aggregation of fluorescence lipid probe with cell surface protein. *J. Cell Biol.* 125:795–802.

20. Dunn, W. A., A. L. Hubbard, and N. N. Aronson Jr. 1980. Low temperature selectively inhibits fusion between pinocytic vesicles and lysosomes during heterophagy of 125I-asialofetuin by the perfused rat liver. *J. Biol. Chem.* 255:5971–5978.

21. Buboltz, J. T., and G. W. Feigenson. 1999. A novel strategy for the preparation of liposomes: rapid solvent exchange. *Biochim. Biophys. Acta.* 1417:232–245.

22. Smith, A. K., J. T. Buboltz, C. H. Spink, and G. W. Feigenson. 2003. Ternary phase diagram of the lipid mixture sphingomyelin/DOPC/cholesterol. *Biophys. J.* 84:372a. (Abstr.).

23. Kahya, N., D. Scherfeld, K. Bacia, and P. Schwille. 2004. Lipid domain formation and dynamics in giant unilamellar vesicles explored by fluorescence correlation spectroscopy. *J. Struct. Biol.* 147:77–89.

24. Veatch, S. L., and S. L. Keller. 2005. Miscibility phase diagrams of giant vesicles containing sphingomyelin. *Phys. Rev. Lett.* 94:148101:1–4.

25. Chiang, Y. W., J. Zhao, J. Wu, Y. Shimoyama, J. H. Freed, and G. W. Feigenson. 2005. New method for determining tie-lines in coexisting membrane phases using spin-label ESR. *Biochim. Biophys. Acta.* 1668:99–105.

26. Meirovitch, E., A. Nayeem, and J. H. Freed. 1984. Analysis of protein-lipid interactions based on model simulations of electron spin resonance spectra. *J. Phys. Chem.* 88:3454–3465.

27. Schneider, D. J., and J. H. Freed. 1989. Calculating slow motional magnetic resonance spectra. *In* Biological Magnetic Resonance, Vol. 8. L. J. Berliner and J. Reuben, editors. Plenum Press, New York. 1–76.

28. Budil, D. E., S. Lee, S. Saxena, and J. H. Freed. 1996. Nonlinear-least-squares analysis of slow-motion EPR spectra in one and two dimensions using a modified Levenberg-Marquardt algorithm. *J. Magn. Reson. A.* 120:155–189.

29. Kar, L., E. Ney-Igner, and J. H. Freed. 1985. Electron spin resonance and electron-spin-echo study of oriented multilayers of L_d-dipalmitoylphosphatidylcholine water systems. *Biophys. J.* 48:569–595.

30. Fajer, P., A. Watts, and D. Marsh. 1992. Saturation transfer, continuous wave saturation, and saturation recovery electron spin resonance studies of chain-spin labeled phosphatidylcholine. *Biophys. J.* 61:879–891.

31. Earle, K. A., J. K. Moscicki, M. Ge, D. E. Budil, and J. H. Freed. 1994. 250-GHz electron spin resonance studies of polarity gradients along the aliphatic chains in phospholipids membranes. *Biophys. J.* 66:1213–1221.

32. London, E. 2005. How principles of domain formation in model membranes may explain ambiguities concerning lipid raft formation in cells. *Biochim. Biophys. Acta.* 746:203–220.

33. Gidwani, A., D. Holowka, and B. Baird. 2001. Fluorescence anisotropy measurements of liquid order in plasma membrane and lipid rafts from RBL-2H3 mast cells. *Biochemistry.* 40:12422–12429.

34. Chiang, Y.-W., Y. Shimoyama, G. W. Feigenson, and J. H. Freed. 2004. Dynamic molecular structure of DPPC-DLPC-cholesterol ternary lipid system by spin-label ESR. *Biophys. J.* 87:2483–2496.

35. Devaux, P. F., and M. Seigneuret. 1985. Specificity of lipid-protein interactions as determined by spectroscopic techniques. *Biochim. Biophys. Acta.* 82:63–125.

36. Ge, M., and J. H. Freed. 1999. Electron-spin resonance study of aggregation of gramicidin in DPPC bilayers and hydrophobic mismatch. *Biophys. J.* 76:264–280.

37. Costa-Filho, A. J., R. H. Crepeau, P. P. Borbat, M. Ge, and J. H. Freed. 2003. Lipid-gramicidin interactions: dynamic structure of the boundary lipid by 2D-ELDOR. *Biophys. J.* 84:3364–3378.

38. Carruthers, A., and D. L. Melchior. 1983. Studies of the relationship between bilayer water permeability and bilayer physical state. *Biochemistry.* 22:5797–5807.

39. Jacobs, R. R., and S. H. White. 1989. The nature of the hydrophobic binding of small peptides at the bilayer interface: implications for the insertion of transbilayer helices. *Biochemistry.* 28:3421–3437.

40. Perochon, E., A. Lopez, and J. F. Tocanne. 1992. Polarity of lipid bilayers. A fluorescence investigation. *Biochemistry.* 31:7672–7682.

41. Sahaf, B., K. Heydari, L. A. Herzenberg, and L. A. Herzenberg. 2003. Lymphocyte surface thiol levels. *Proc. Natl. Acad. Sci. USA.* 100:4001–4005.

42. Zachowski, A. 1993. Phospholipids in animal eukaryotic membranes: transverse asymmetry and movement. *Biochem. J.* 294:1–14.

43. Pomorski, T., S. Hrafnsdottir, P. F. Devaux, and G. van Meer. 2001. Lipid distribution and transport across cellular membranes. *Semin. Cell Dev. Biol.* 12:139–148.

44. Hao, M., S. X. Lin, O. J. Karylowki, D. Wustner, T. E. McGraw, and F. R. Maxfield. 2001. Vesicular and non-vesicular sterol transport in living cells. The endocytic recycling compartment is a major sterol storage organelle. *J. Biol. Chem.* 277:609–617.

45. Marsh, D. 1989. Experimental methods in spin-label spectral analysis. *In* Biological Magnetic Resonance. Spin Labeling: Theory and Application, Vol. 9. L. J. Berliner and J. Reuben, editors. Plenum Press, New York. 255–303.

46. Jost, P. C., O. H. Griffith, R. A. Capaldi, and G. A. Vanderkooi. 1973. Evidence for boundary lipid in membranes. *Proc. Natl. Acad. Sci. USA.* 70:480–484.

47. Knowles, P. F., A. Watts, and D. Marsh. 1979. Spin-labeled studies of lipid immobilization in dimyristoylphosphatidylcholine-substituted cytochrome oxidase. *Biochemistry.* 18:4480–4487.

48. Marsh, D., and A. Watts. 1982. Spin labeling and lipid-protein interactions in membranes. *In* Lipid-Protein Interactions. P. C. Jost and O. H. Griffith, editors. John Wiley & Sons, New York. 53–126.

49. Griffith, O. H., D. A. McMillen, J. F. W. Keana, and P. C. Jost. 1986. Lipid-protein interactions in cytochrome c oxidase. A comparison of covalently attached phospholipids photo-spin-label with label free to diffuse in the bilayer. *Biochemistry*. 25:574–584.

50. Costa-Filho, A. J., Y. Shimoyama, and J. H. Freed. 2003. A 2D-ELDOR study of the liquid ordered phase in multilamellar vesicle membranes. *Biophys. J.* 84:2619–2633.

51. Pike, L. J. 2004. Lipid rafts: heterogeneity on the high seas. *Biochem. J.* 378:281–292.

52. Holowka, D., and B. Baird. 1983. Structural studies on the membrane-bound immunoglobulin E-receptor complex. 1. Characterization of large plasma membrane vesicles from rat basophilic leukemia cells and insertion of amphipathic fluorescent probes. *Biochemistry*. 22:3466–3474.

53. Fastenberg, M. E., H. Shogomori, X. Xu, D. A. Brown, and E. London. 2003. Exclusion of a transmembrane-type peptide from order-lipid domain (rafts) detected by fluorescence quenching: extension of quenching analysis to account for the effects of domain size and domain boundaries. *Biochemistry*. 42:12376–12390.

54. Anderson, R. G. W., and K. Jacobson. 2002. A role for lipid shells in targeting proteins to caveolae, rafts, and other lipid domains. *Science*. 296:1821–1825.

55. Holowka, D., E. D. Sheets, and B. Baird. 2000. Interactions between Fc(epsilon)RI and lipid rafts components are regulated by the actin cytoskeleton. *J. Cell Sci.* 113:1009–1019.

56. Kusumi, A., I. Koyama-Honda, and K. Suzuki. 2004. Molecular dynamics and interactions for creation of stimulation-induced stabilized rafts from small unstable steady-state rafts. *Traffic*. 5:213–230.

57. Simons, K., and L. C. V. Winchil. 2004. Model systems, lipid rafts, and cell membranes. *Annu. Rev. Biophys. Biomol. Struct.* 33:269–295.

58. Silvius, J. R. 2003. Role of cholesterol in lipid raft formation: lessons from lipid model systems. *Biochim. Biophys. Acta*. 1610:174–183.

59. Ipsen, J. H., G. Karlström, O. G. Mouritsen, H. Wennerström, and M. J. Zuckermann. 1987. Phase equilibria in the phosphatidylcholine-cholesterol system. *Biochim. Biophys. Acta*. 905:162–172.

60. Crane, J. M., and L. K. Tamm. 2004. Role of cholesterol in the formation and nature of lipid rafts in planar and spherical model membranes. *Biophys. J.* 86:2965–2979.

61. Mayor, S., and M. Rao. 2004. Rafts: scale-dependent active lipid organization at the cell surface. *Traffic*. 5:211–212.

62. Shin, Y. K., U. Ewert, D. E. Budil, and J. H. Freed. 1991. Microscopic versus macroscopic diffusion in model membranes by electron spin resonance spectral-spatial imagine. *Biophys. J.* 59:950–957.

63. Freed, J. H. 1994. Field gradient ESR and molecular diffusion in model membranes. *Annu. Rev. Biophys. Biomol. Struct.* 23:1–25.

64. Veatch, S. L., I. V. Polozov, K. Gawrisch, and S. L. Keller. 2004. Liquid domains in vesicles investigated by NMR and fluorescence microscopy. *Biophys. J.* 86:2910–2922.

65. Elliot, R., I. Szleifer, and M. Schick. 2006. Phase diagram of a ternary mixture of cholesterol and saturated and unsaturated lipids calculated from a microscopic model. *Phys. Rev. Lett.* 96:098101:1–4.